34th EUROPEAN ROTORCRAFT FORUM

Session: Acoustics

ACTIVELY CONTROLLED ROTOR: AERODYNAMIC AND ACOUSTIC BENEFIT FOR THE HELICOPTER TODAY AND TOMORROW

by

A. Altmikus, A. Dummel, R. Heger, D. Schimke*

*EUROCOPTER DEUTSCHLAND GmbH, 81663 München, Germany

SEPTEMBER 16 - 18, 2008
LIVERPOOL
UNITED KINGDOM

ACTIVELY CONTROLLED ROTOR: AERODYNAMIC AND ACOUSTIC BENEFIT FOR THE HELICOPTER TODAY AND TOMORROW

A. Altmikus, A. Dummel, R. Heger, D. Schimke*

* Eurocopter Deutschland GmbH, Munich, Germany

Abstract

Active rotor concepts are of high interest in today's helicopter research due to their potential in noise, required rotor power and vibration reduction. This paper focuses on the "aerodynamic" benefits noise and performance.
In the frame of various national [ADASYS, LARS, INROS] and European [FRIEND-COPTER] research projects active rotors with different actuation principles have been investigated and developed until certain technology readiness levels. The most advance is most certainly the discrete piezo activated flap that is flight tested since its maiden flight in September 2005 at Eurocopter Deutschland [4]. Other technologies are the so called active trailing edge, and the active twist concept developed in FRIENDCOPTER.
The designs have been based and numerically assessed on the ATR-A rotor, which is a modern hingeless fibre reinforced polymer rotor used on the EC145. Its advanced blades feature a non-rectangular plan-form and a parabolic blade tip. In order to numerically evaluate the potential of the concepts with respect to the expected benefits for noise and performance, various methods have been applied on different levels of modelling. The active control strategy for all investigated cases is based on 2/rev control laws with varying amplitude and phase shift.
Acoustic characteristics of the isolated main rotor have been investigated in detailed numerical simulations. Special focus was given to the prediction of BVI noise in stabilised descent flight conditions for various 2/rev control settings. Based on the aerodynamic forces obtained from this simulation, the corresponding noise contours on ground were calculated using a Ffowcs Williams-Hawkings acoustic code.
Performance benefit has been investigated numerically by an aeromechanic code and by periodically coupling this code with a high resolution CFD method for a discrete trailing edge servo flap and a continuous active trailing edge deformation. The technical feasibility of the later technology has been proven by a full scale hardware specimen in component testing.
Derived from the rich experience from the research programmes mentioned above and industrial constraints some trends can be derived for the future developments, which include a compromise between maximum benefits for the helicopter and well defined steps towards an industrial realisation.

Nomenclature

Symbols

μ	Advance ratio
Ma	Mach number
θ_0	Collective pitch angle [°]
θ_{1c}	Longitudinal cyclic pitch [°]
θ_{1s}	Lateral cyclic pitch [°]
α_q	Rotor shaft angle [°]
Ψ	Azimuth angle
φ	Phase angle of the HHC-law
C_T	Thrust coefficient
C_Q	Torque coefficient
C_{Mx}	Rotor mast roll moment coefficient
C_{My}	Rotor mast pitch moment coefficient
C_nMa^2	Sectional normal force coefficient
C_mMa^2	Sectional pitching moment coef.
$C_{Fz}Ma^2$	Sectional thrust coefficient (in z-direction of rotating system)
$C_{Fy}Ma^2$	Sectional drag coefficient (in y-direction of rotating system)
$C_{Mx}Ma^2$	Sectional moment coefficient (around x-direct. of rotating system)
ENPL	Effective perceived noise level [EPNdB]
L_A	A-weighted sound pressure level [dB(A)]
L_p	Sound pressure level [dB]
N	Number of harmonic
p	Sound pressure level [Pa]
PNL	Perceived noise level [PNdB]
PNLT	Tone corrected perceived noise level [TPNdB]

Trim numbering

- The initial HOST trim is denoted as 0^{th} trim.
- The FLOWer calculation following the n^{th} HOST trim is denoted as n^{th} FLOWer trim.

Acronyms

ADASYS	Adaptives Dynamisches System für Hubschrauber
APSIM	Acoustic Prediction System based on Integral Method (by DLR)
ATE	"Soft" Active Trailing Edge Deformation
ATR-A	Advance Technology Rotor A
ATW	Active Twist
BVI	Blade Vortex Interaction
CFD	Computational Fluid Dynamics
CAMRAD	Comprehensive Analytical Model of Rotorcraft Aerodynamics and Dynamics
DSF	Discrete Trailing Edge Servo Flap
DLR	Deutsches Zentrum für Luft- und Raumfahrt e.V.
DOF	Degree of Freedom
FAA	Federal Aviation Administration
FLOWer	RANS solver (by DLR)
FRIEND COPTER	Environmentally Friendly Helicopter
HOST	Helicopter Overall Simulation Tool
IBC	Individual blade control
ICAO	International Civil Aviation Organization
INROS	Innovative Rotorsysteme
LARS	Lagerloses Aktives Rotorsystem
TRL	Technology Readiness Level

Introduction

Today, the principle fields for improvements of the unsteady aerodynamics of main rotors are noise, required power and vibrations in the full flight envelope of the helicopter. Noise and performance are fully aerodynamically driven phenomena.

Noise emissions most annoyingly occur in steady approach flight under a certain glide slope angle when preceding blade vortices interact parallel with the following blade. The typical BVI noise is shed.

Performance becomes an important issue in high speed forward flight when the wave drag of the advancing blade tip is rising due to high Mach numbers seen by the blade and large stalled regions on the retreating blade.

Since many years now EUROCOPTER tackles theses conditions by investigating active devices in the rotating frame of the main rotor. EUROCOPTER historically started with hydraulically activated blade root IBC on a BO105. In 1998, the first time the reduction of BVI noise by IBC could be demonstrated in flight together with a local measurement of the typical BVI pressure distribution [1]. Several publications in the following proved the potential of a 2/rev control input as the most efficient control strategy for noise and performance because this frequency can be quite independently used from the typically used frequencies for vibration reduction.

Today, a change to piezo activated servo trailing edge flaps integrated in the outboard region of the blades on the BK117 is realised. The maiden flight took place in 2005 and was extensively reported in [4]. For both technologies significant vibration and noise benefits have been reported [2], [3], [5]. However, on subsystem level EUROCOPTER always strived for further optimisation and technical alternatives. The one answer is a further improvement of the discrete active trailing edge flap. The second answer was to afford investigation of yet other three technologies which promise additional aerodynamic benefit. The active trailing edge (ATE), offering a continuous flap like deformation and the full blade active twist (ATW) offering a completely undisturbed aerodynamic blade shape. Technology Overview

Individual Blade Root Control

The first IBC demonstrator operated by ECD was the BO105 S1 helicopter using electro-hydraulic blade pitch actuators provided by ZF Luftfahrttechnik (ZFL) which replaced the pitch links in the rotating frame, see Figure 1. For safety reasons the blade pitch authority of the actuators was limited by hardware stops to 1.1 deg. Although the authority was further reduced by software limits, the available IBC blade pitch amplitude proved to be sufficient for impressive BVI noise reduction in descent flight [2], [6] and for significant vibration reduction in level flight [7].

Figure 1: BO105 S1 IBC demonstrator in flight

Discrete Trailing Edge Servo Flap (DSF)

Although the electro-hydraulic system of the BO105 behaved well during the experimental campaign, a promising actuation concept for future applications was seen in piezo-actuated trailing edge flaps. For the new experimental rotor system a BK117 was selected as test bed. Concerning the main rotor system, it should be noted that the rotor hub of type Boelkow is the same for both helicopters. Table 1 gives a comparison of the test helicopters.

BO105 S1	BK117 S7045
Rotor radius 4.9m	Rotor radius 5.5m
Nominal TOW 2300kg	Nominal TOW 3000kg
Four bladed hingeless rotor (type Boelkow)	Four bladed hingeless rotor (type Boelkow)
Rectangular blade geometry (NACA 23012)	Advanced blade geometry (OA3 series)
IBC by blade root actuation	IBC by trailing edge servo flaps

Table 1: Comparison of IBC test beds operated by ECD.

Flap Location and Dimensions

An important design parameter is the radial position of the flap. Parametric studies revealed that for BVI noise reduction purposes the flap should be shifted as close as possible to the blade tip. Due to the blade tip design with a swept back planform, the outboard end of the flap was limited to radius station 4.9 m (0.89R). In the contrary the most beneficial location for vibration control is in the mid range span at 4 m (0.73R). Flap chord and the torsion stiffness of the blade impact the blade response as well. Lower blade torsion stiffness and smaller flap chords support the servo effect of the flap and helps to limit the needed actuator power [8].

Rotor Blades

Basis for the implementation of the flaps was the EC145 main rotor. The planform of the blades has an inboard tapering and features a swept back parabolic tip. The design of the blade was modified to integrate the active trailing edge flaps with characteristics as shown in Table 2. The flap system consists of three identical units with an individual length of 0.3 m. Dedicated studies revealed that one pair of the available piezoelectric actuator is able to run a flap of 300 mm extension and a chord of 50 mm. The trailing edge of the blade was cut out and the foam used as support between the upper and lower blade skin was substituted by a flat box made from carbon fibre. The box is open at the aft side. After inserting the units into the blade all the parts are screwed and sealed to ensure the stiffness and strength requirements of the blade, as well as the protection of the flap actuation system against humidity.

Chord	0.05m, 15%
Max length	0.9m
Radius station	3.8m – 4.7m
3 Units	0.3m each
Max. flap angle	+/- 10 deg

Table 2**:** Flap geometry

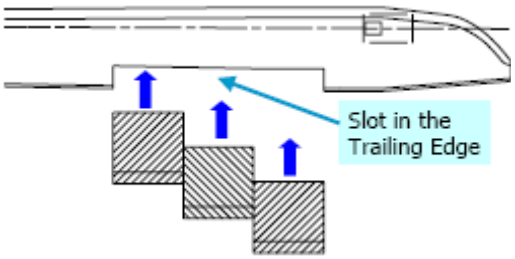

Figure 2: Installation of the flap units from the trailing edge side

One pair of piezoelectric actuators located at a most forward chordwise position act via tension rods on the flap (see Figure 3).

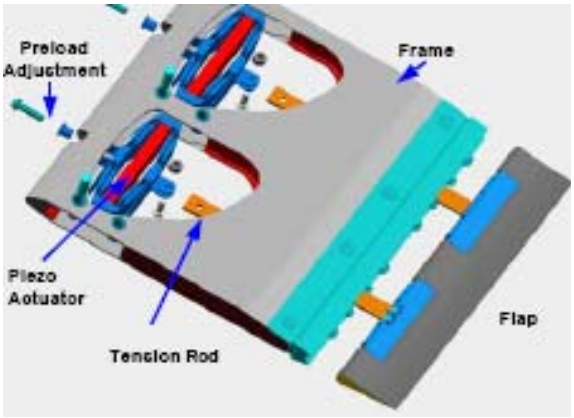

Figure 3: Flap unit

The blade segment containing the flaps was tested in a bending-machine shown in Figure 4. While the specimen is clamped on the left hand side, it is displaced on the opposite side. It survived the fatigue test with a level far above the flight limit loads. One active flap unit was operated during the tests to check a proper function even when the blade was bent in an extreme manner. A tension load of 107 kN simulating the centrifugal force at nominal rotor speed was superimposed on bending and torsion moments.

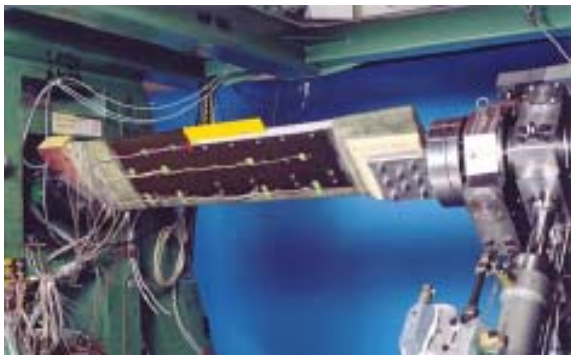

Figure 4: Blade specimen with active flap during fatigue test

After whirl tower testing of the active rotor and securing a save operation of the aircraft on ground which includes the balancing of the rotor and checking of ground resonance stability the system was activated the first time. The helicopter became airborne with some hover flights, followed by air resonance tests and checks of the handling qualities. Although blade pendulum absorbers or other vibration suppression means were not installed the vibration level was rated acceptable by the crew. The official first flight of a helicopter with active trailing edge flaps took place in September 2005. The airborne demonstrator is depicted in Figure 5.

Figure 5: First flight of the BK117 S7045 with active trailing edge flaps

Active Trailing Edge (ATE)

Although the discrete piezo-active system of the BK117 behaves well during the experimental campaigns since the maiden flight, the mechanical complexity of the design gave rise to new conceptual ideas.

Figure 6: 2½D laboratory specimen

One idea developed in FRIENDCOPTER is a trailing edge deformation by distributed actuation. The concept consists of a polymorph bender (Figure 7) attached to an upstream positioned interface at the torsion box closure (Figure 8) and a re-installed airfoil shape by a light weight and flexible filler material (Figure 6).

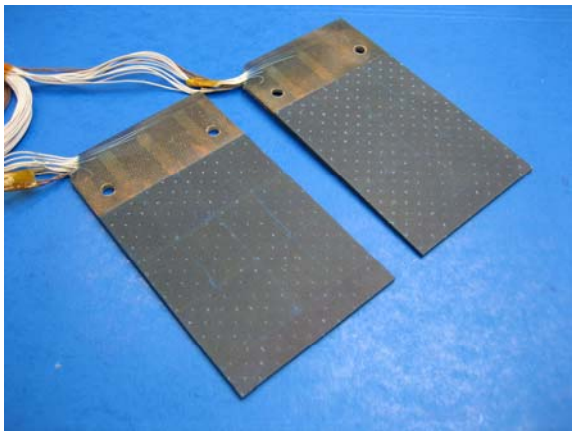

Figure 7: Polymorph bender modules

The lay-up of the bending modules has been optimised for maximum aero-servo-elastic authority [9], [10], [11], [12]. Parameters subject to variation are e.g. the thickness of the electrically insulated glas fibre reinforced polymer carrier layer, the piezo thickness and a chord wise thickness diminution toward the free end.

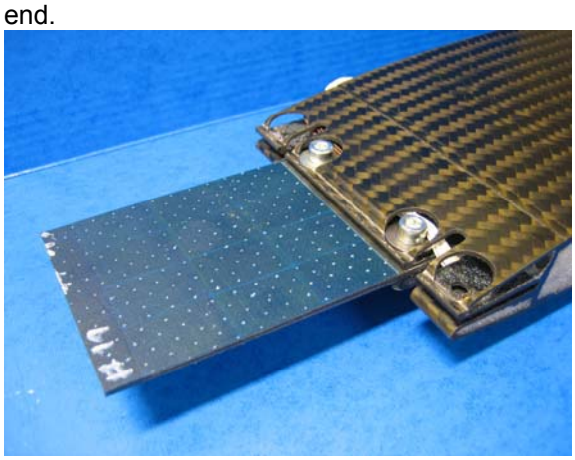

Figure 8: Bender module attached to an interface at the torsion box closure

As can be seen form Figure 8 the bender module can be regarded as one-sided clamped beam. In order not to loose too much deformation in the interface, is has been optimised to support the introduced bending moments.
At the same time the interface is highly loaded by lead-lag bending moments and centrifugal loads of the rotor blade. Since piezo patches do not support related tensile strain in this area, specific relief cuts are conceived to limit this

strain. These cuts have been systematically optimised to find the best length to width ratio [13]. Of course the integrity of the fundamental blade strength was assured and preserved as for a conventional passive blade.

The resulting active trailing edge deformation compared to the active flap deflection (oversized) is shown in Figure 9. The discrete flap deflection leads to a kink in the airfoil contour. The active trailing edge has a continuous shape with an increased tab tangent.

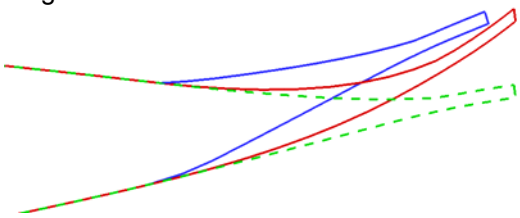

Figure 9: Comparison of airfoil shape in the trailing edge region: green - original airfoil, blue - discrete flap, red - active trailing edge

Following the stress and strength driven actuator and interface lay-out the resultant outline of the rotor blade with integrated piezos is investigated by three dimensional finite element analyses. Subsequently, a full scale blade segment is designed preparing the specimen manufacture in detail. The section is a cut out of the EC145 blade described in the section of the DSF. The approximate dimensions can be judged from Figure 10. After manufacture of the required tooling the existing blade form is used to lay-up the segment.

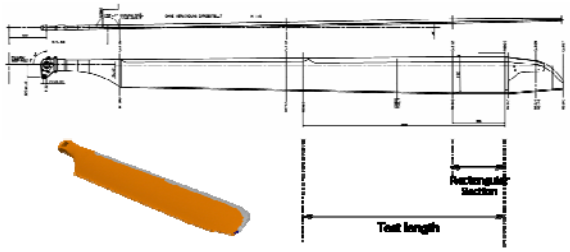

Figure 10: Full scale specimen definition

It is planned to conduct an industrial component test of this main rotor blade segment with integrated active modules. Static and dynamic strength of the modified blade structure, the functionality and the strength of the piezo modules and finally, the effect of the filling material on attainable trailing edge deflection shall be examined. Combined centrifugal force, flap and lead-lag moments and torsion are applied during the test. A schematic of the test set-up is depicted in Figure 11.

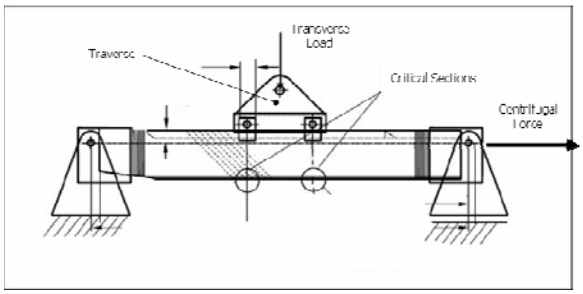

Figure 11: Schematic of the test set-up for lead-lag

The finished specimen is instrumented with strain gauges for flap, lead-lag bending and torsion moments. Additional singular strain gauges measure the interface strain at the middle position of two active modules. Furthermore the bender modules themselves are instrumented with embedded strain gauges to record the remaining tensile strain directly on the modules. The calibration values have been used to validate the 3D finite element analysis and a good correlation has been found between measurement and numeric prediction [13].

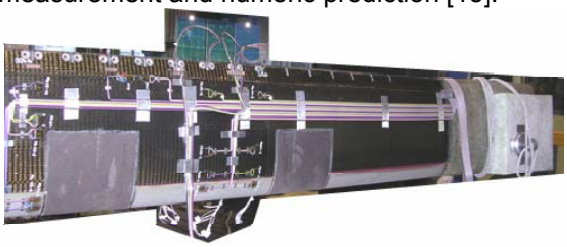

Figure 12: Calibration set-up

Active Twist

The second FRIENDCOPTER technology developed is the full blade active twist (ATW) studied in model scale. The objective is to enable an n/rev active twist actuation with enough authority to realise significant noise, vibration and performance benefits. A model rotor blade with a 2.1m span is designed and manufactured in the frame of FRIENDCOPTER [14], [15].

Numerical Methods

In complement to the hardware design and manufacture the benefits are numerically investigated. The used tools at EUROCOPTER are briefly described below.

Aeromechanics model 1 (CAMRAD)

For the aeromechanic simulation which served as basis for the acoustic post processing the comprehensive rotorcraft code CAMRAD II [16], [17] was used. Providing trimmed blade response based on an analytical structural rotor model in combination with local unsteady

aerodynamics and an elaborated multiple trailer free wake model the blade element based software is well suited as input for an industrially efficient rotorcraft BVI noise prediction approach.

Acoustic Post Processing (APSIM)

The acoustic calculation tool APSIM developed by DLR represents a state-of-the-art noise prediction code based on the Ffowcs Williams-Hawkings equation [18].
The acoustic model has been extensively validated with data from the wind tunnel test campaigns HART II and HeliNovi and with flight test measurements [19], [20], [21].

Aeromechanics model 2 (HOST)

The EUROCOPTER flight mechanics tool HOST [16] represents a computational environment for simulation and stability analysis of the complete helicopter system. It enables the study of single helicopter components like isolated rotors as well as complete configurations with related substructures.
As a general purpose flight mechanics tool, HOST is capable of trimming the rotor based on a lifting-line method with 2D airfoil tables. Additional interpolation is preformed for a flap in the polar curves depending on the flap angle. The airfoil tables are measured or numerically created. For the DSF and the ATE the numerical approach was used. Figure 13 illustrates the difference between the active trailing edge and the discrete servo flap at Ma=0.6 for nominal amplitude taking into account aeroelastic authority losses on the device. The same trailing edge displacement has been set leading to different flap or secant angles for the DSF and the ATE, respectively.
Since all active rotor concepts described above directly or indirectly induce elastic torsion and excite via cross-couplings other elastic blade modes the elastic motion is of great importance for a reliable prediction.
The elastic blade model in HOST considers the blade as a quasi one-dimensional Euler-Bernoulli beam. It allows for deflections in flap and lag direction and elastic torsion along the blade axis. In addition to the assumption of a linear material law, tension elongation and shear deformation are neglected. However, possible offsets between the local cross-sectional centre of gravity, tension centre and shear centre are accounted for, thus coupling bending and torsion degrees of freedom DOFs.

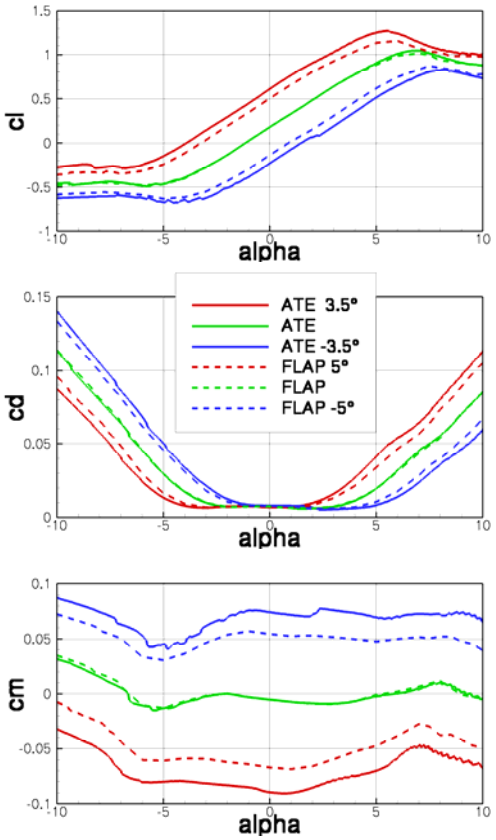

Figure 13: Comparison of polar curves for ATE and DSF at Ma=0.6 for the nominal deflection

The blade model is based on a geometrically non-linear formulation, connecting rigid segments through virtual joints [23]. At each joint, elastic rotations are permitted about the lag, flap and torsion axes. Since the use of these rotations as DOFs would yield a rather large system of equations, the number of equations is reduced by a modal approach. A limited set of mode-like deformation shapes together with their weighting factors are used to yield a deformation description.

Therefore, any degree of freedom can be expressed as,

$$h(r,\psi) = \sum_{i=1}^{n} q_i(\psi) \cdot \hat{h}_i(r) \qquad (1)$$

where n is the number of modes, q_i the generalized coordinate of mode i (a function of the azimuth angle ψ), and $\hat{h}_i$ is the modal shape (a function of the radial position r).

Aerodynamic model (FLOWer)

In the present study FLOWer [24] has been used for the aerodynamics, which is available at ECD through the cooperation with DLR (Deutsches Zentrum für Luft- und Raumfahrt e.V.). FLOWer solves the three-dimensional,

unsteady Euler or Reynolds-averaged Navier-Stokes equations in order to analyze the flow field around the helicopter rotor. These equations are formulated in a hub attached, non-inertial, rotating frame of reference, with explicit contributions of centrifugal and Coriolis forces. See [25] for details of the algorithm!
The discretisation of space and time is separated by the method of lines using a cell-vertex or cell-centred finite volume formulation. Spurious oscillations of the central difference scheme are suppressed by first and second order artificial dissipation. The time integration makes use of the dual time stepping technique with a second order implicit time integration operator [26].
FLOWer features the Chimera-technique [27] allowing for arbitrary relative motion of aerodynamic bodies. Body fitted grids around each blade are embedded in a background grid (Figure 14), in which the blade vortex sheets are convected from one blade grid to the next. The elastic deformation of the blade can be introduced into the body fixed mono-block grids by an algebraic deformation method for OH- and CH-topologies [28].

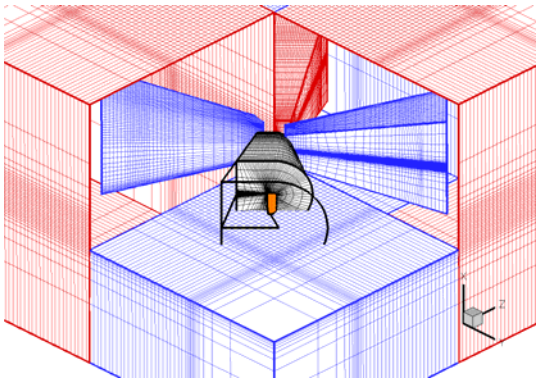

Figure 14: Chimera grid set-up

Periodic Coupling

The iterative coupling scheme used for the present work basically corresponds to the technique used in [16], [30], [29]. HOST uses CFD loads to correct its internal 2D aerodynamics and re-trims the rotor. The blade dynamic response is introduced into the CFD calculation in order to obtain updated aerodynamic loads. This cycle is repeated until the CFD loads match with the blade dynamic response evoked by them. A criterion for this converged state is given by the change in the free controls with respect to the preceding cycle. Convergence has been reached after the changes in the controls have fallen below this imposed limit. All coupled calculations of this paper have been trimmed until the change in the free controls θ_0, θ_{1c}, θ_{1s} is less than 0.005°.

Grid Deformation

In order to correctly model the dynamic behaviour of the rotor blade in the CFD solver, the blade must be deformed according to the output of the preceding HOST calculation. This requires the reconstruction of the blade elastic axis and its elastic twist for a given azimuth angle. The same strategy as used in HOST was adopted to describe the blade deformation (see above). Further details concerning the global grid deformation can be found in [30]
In the case of the active rotor, the flap deflection is introduced as a local grid deformation of the blade surface in the flap region. As the flap is modelled as a pure grid deformation the slit at the inner and outer flap boundary cannot be reproduced exactly (s. Figure 15).

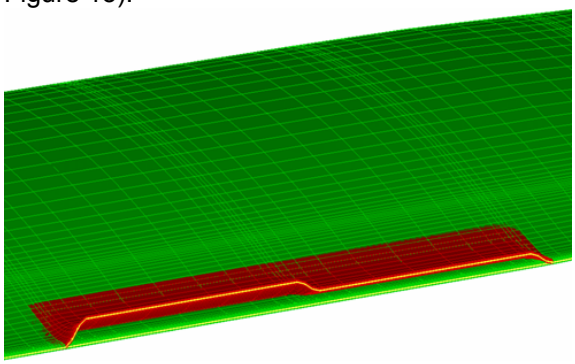

Figure 15: Local grid deformation for flap and active trailing edge modelling; green – passive blade, red – active trailing edge deflection.

However, all relevant consequences of a flap deflection (e.g. influence on blade surface pressure distribution, jump in circulation, vortex shedding etc.) are correctly modelled, thus this flaw in the modelling is acceptable. At the flap boundaries the flap deflection is reduced to zero within a certain smoothing range. The extent of this smoothing area can be minimized by radial clustering of the blade grid in the relevant regions. The flap model which has been introduced into FLOWer is able to model several flap segments which can be individually deflected using a (higher) harmonic control law. In the case of the active rotor the deformation process due to weak coupling acts upon a pre-deformed blade surface which contains the deflections of the flap segments.

Benefit in Simulation and Experiment

Acoustics

Acoustic Test Case

The noise benefit calculation for the active trailing edge concept developed in

FRIENDCOPTER was performed for a 6 deg descent flight at a moderate velocity of 65 kts. This flight condition represents the certification approach case according to ICAO and FAA regulations and is therefore a good indicator for the industrially significant obtainable noise benefit by means of BVI noise reduction through 2/rev control.

The aeromechanic simulation was performed using a CAMRAD II model of the active ATR-A main rotor. Following the experience of previous noise validation campaigns, the rotor was trimmed for thrust, lateral and longitudinal mast moment by adaptation of the free controls θ_0, θ_{1c}, θ_{1s}.

For the passive and the active rotor calculations the corresponding attitude angles as well as the shaft angle α_q=*-5.0°* were identical.

The trim procedure was conducted with an azimuth resolution of $\Delta\Psi$=*10°* that was refined afterwards to $\Delta\Psi$=*2.5°* using the post trim ability provided by CAMRAD II.

The in reality continuous active trailing edge was approximated in the aeromechanic model with 15 discrete trailing edge flap elements ranging from 56.4% to 95% blade radius.

A pure 2/rev higher harmonic control law was investigated for the active control with a trailing edge flap amplitude of A_0 = *2.5°* and a simulation step size for the phase angle variation of $\Delta\varphi$ = *15°* from φ = *0°* to φ = *165°* according to the following formula:

$$A(t) = A_0 \cdot \cos(2 \cdot \Omega \cdot t - 2 \cdot \varphi) \qquad (2)$$

The obtained aerodynamic lift distribution served as input for the aeroacoustic FWH-code APSIM. For the acoustic calculations an array of 441 microphones equally distributed on a 1000m x 1000m plane located 150m below the rotor was chosen to capture the relevant directivity information. The microphone system for the present investigation was fixed relative to the rotor system. Therefore no time integrated noise metrics like SEL or EPNL are derived.

The acoustic results encompass the simulated pressure time history on each microphone position for one rotor revolution as well as the corresponding frequency spectra and global noise values.

Acoustic Results

In this section, the calculated acoustic results for the passive rotor as well as for the active trailing edge phase variation are presented. The acoustically best setting is identified and compared in detail with the passive baseline concept.

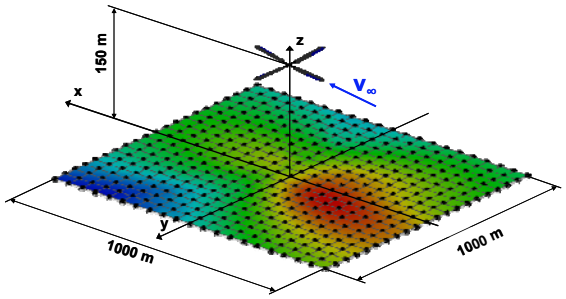

Figure 16: Microphone array for acoustic footprint calculation in APSIM

In Figure 17 the difference of the maximum global noise levels for the different phase angles of the 2/rev input relative to the passive baseline case are presented.

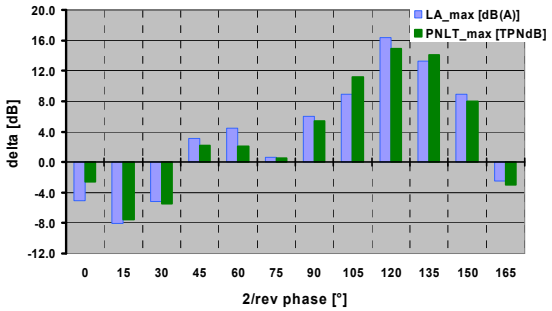

Figure 17: Acoustic benefit for different 2/rev phase angles

Evidently a similar behaviour of the noise level as a function of control phase angle can be observed for the L_A and the PNLT metric with slightly higher amplitudes in the L_A variation. The maximum reduction of about -8 dB(A) or -7.5 TPNdB is achieved for a phase angle of φ = *15°*. The loudest setting is represented by a phase angle of φ = *120°* with an increase of 16 dB(A) or 15 TPNdB respectively.

In the following detailed investigation the passive rotor is referred to as baseline case and the best 2/rev setting identified above as φ = *15°* is henceforth called the minimum noise case.

In Figure 18 and Figure 19 the calculated noise footprints for the baseline and the minimum noise test case are presented in TPNdB for a rotor flying in negative x direction. The colour scale is identical for both plots.

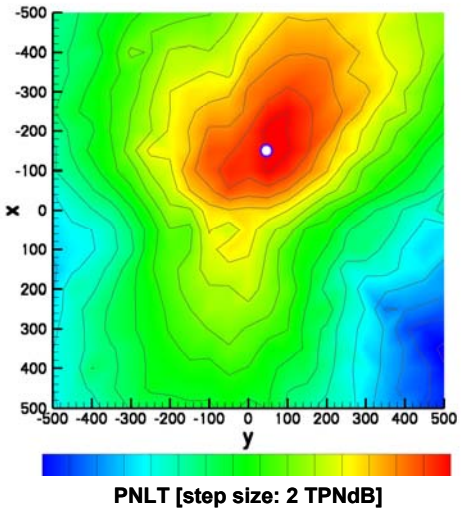

Figure 18: PNLT footprint baseline case

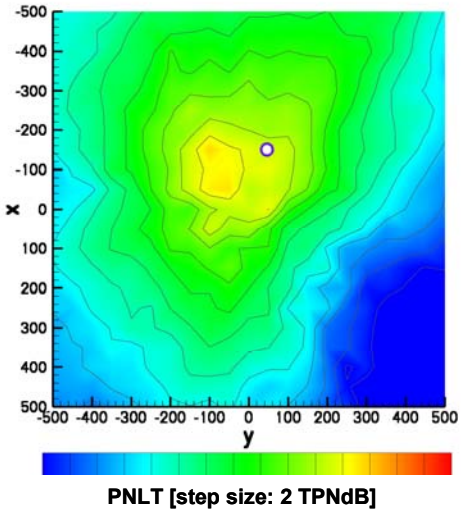

Figure 19: PNLT minimum noise case ($\varphi = 15°$)

The passive rotor simulation yields a noise directivity with the area of maximum noise centred at 200 m upstream and 75 m towards the advancing side. Interestingly the location of the loudest area for the active minimum noise setting is not so different but extends a little more towards the retreating side. The most eminent reduction appears in the upper right corner presumably an effect of decreased vortex interaction on the advancing side of the blade. Nevertheless there is also a non-negligible noise reduction in the lower half of the footprint. This directivity suggests a positive effect also on the retreating side of the blade. Evidently the 2/rev input actually decreases the noise over the complete directivity range under investigation, with the global shape of the footprint remaining rather unchanged.

In both footprints the microphone receiving the maximum noise in the baseline case is marked with a white dot. The calculated pressure time histories at this microphone show a clear reduction of the impulsive change in sound pressure level for the active rotor system compared with the passive concept (Figure 20).

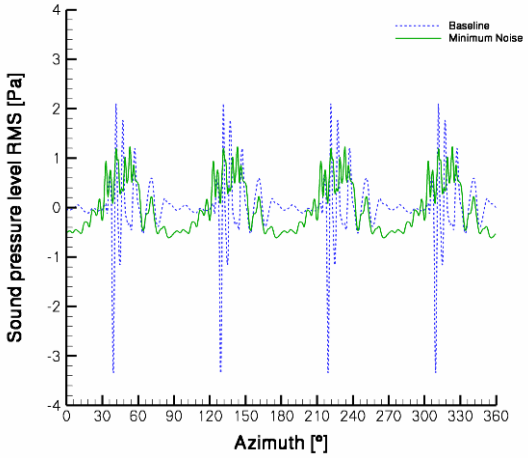

Figure 20: Sound pressure time history for loudest microphone location

In order to analyse the noise decrease on frequency level, the linear narrow band spectra for both test cases are compared exemplarily on this microphone (Figure 21).

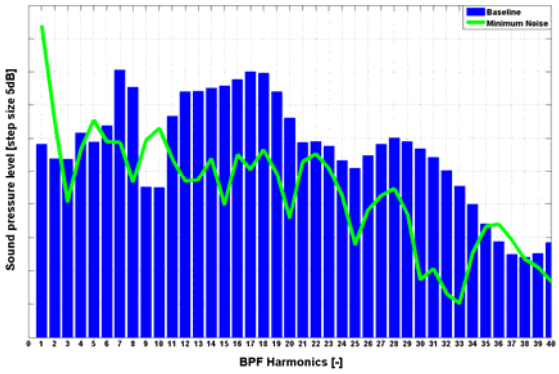

Figure 21: Frequency spectra for loudest microphone location

Clearly the higher harmonic frequency content of the noise spectrum (6^{th} to 40^{th} BPF) typically produced by BVI on the rotor blades is strongly reduced by the active control of the trailing edge. In line with observations during previous flight tests at ECD with the discrete active rotor flaps, the noise emission at the fundamental blade passing frequency is strongly increased by the higher harmonic input. Due to the very low weighting factor for this frequency the effect is negligible on the global noise level in both L_A and PNLT. Nevertheless it is an important aspect for the layout of higher harmonic control laws based on acoustic sensor feedback for realisation in flight.

Apart from the analysis of the tonal narrow band spectra a look on the less detailed third octave spectra gives an even clearer picture (Figure 22).

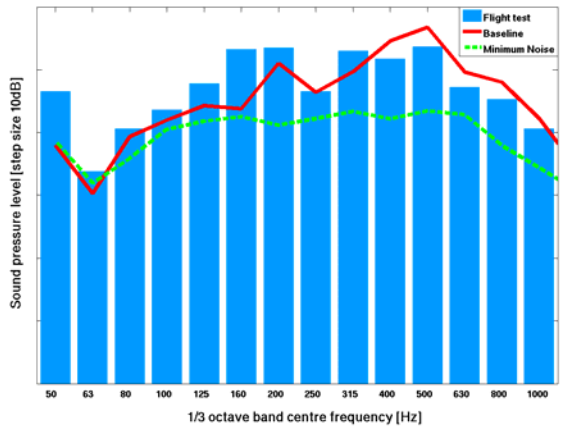

Figure 22: Third octave spectra

The third octave spectrum at PNLTM from a certification approach flight centre microphone is displayed together with the predicted values for baseline and minimum noise case at the same emission angle (distance scaled to the flight test conditions and starting at 50Hz according to the noise certification procedure).
Obviously the global spectral shape is quite reasonably predicted for the baseline case compared to the flight test results without any model tuning applied. Considering the spectral scattering typically observed in acoustic flight test measurements and the tail rotor contribution in the flight test data, the blind prediction accuracy seems very promising. Furthermore the simulated reduction of the higher harmonic peaks at about 200Hz and between 300 and 600Hz with the active control can be easily recognised.

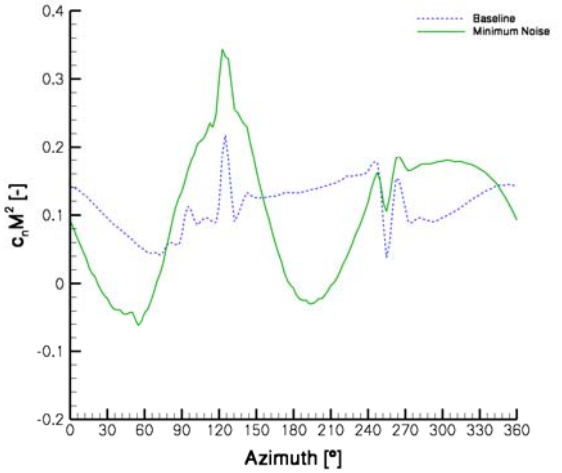

Figure 23: Sectional normal force coefficient at 87% radius

Regarding the sectional normal force distribution at for example 87% radius for one rotor revolution (Figure 23) the effect of reducing the BVI related pressure fluctuations on the advancing as well as on the retreating side through the 2/rev input is clearly visible.
The distribution of the variation of the sectional normal force coefficient over the rotor disk is given for the baseline case (Figure 24) and the minimum noise case (Figure 25).

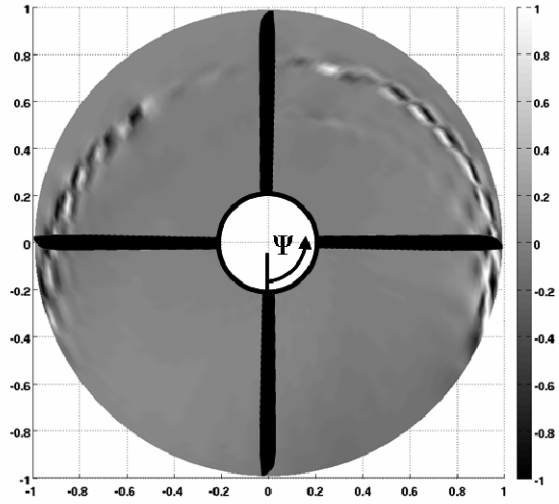

Figure 24: Normal force variation $\delta c_n M^2/\delta\psi$ over rotor disk - baseline

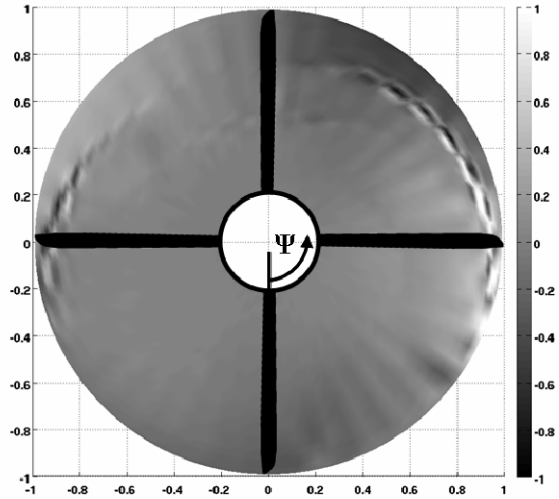

Figure 25: Normal force variation $\delta c_n M^2/\delta\psi$ over rotor disk – minimum noise case

The gray scale shading of the plot easily reveals the presence of areas with high aerodynamic load fluctuations most pronounced at the outer radial blade sections for the baseline case (Figure 24). A comparison with the equivalent distribution for the minimum noise case (Figure 25) shows, that the

amplitude is remarkably diminished by the 2/rev control for the minimum noise configuration. The reduction is most obvious on the retreating side at an azimuth range from about 230° to 250°.
Furthermore there is a significant peak reduction on the advancing side around 70° to 90° azimuth at the blade tip region though less evident in the 2D presentation.
Aside from this the more inboard region with smaller load fluctuations identifiable for the baseline case between 90° and 180° azimuth is almost completely suppressed by the 2/rev control.
Since the aerodynamic loading distribution is the input for the acoustic post processing, the decreased load fluctuation over time is naturally directly correlated with the reduced noise levels calculated by APSIM.
Therefore the reduction in the noise footprints seems to be caused mainly by the reduction of the blade loading due to decreased vortex interaction on the advancing side but also though less pronounced on the retreating side of the rotor.

Summary and outlook

The illustrated calculation results represent a promising approach towards an industrially useable acoustic tool chain for the acoustic assessment and optimisation of modern rotor systems in early phases of the design process.
Concerning the impressively high calculated noise reduction potential for the isolated rotor of up to 7.5 TPNdB is has to be noted that this theoretical value derived for an ideal flight condition cannot be expected to be achieved in flight test measurements due to numerous reasons like

- Scattering of the tip path plane attitude in flight and the resulting unstable wake geometry
- Presence of tail rotor and engine as additional noise sources unaffected by main rotor HHC
- Generally low spatial resolution of the acoustic measurements due to limited number of microphones

In order to quantify the noise benefit under realistic conditions, the predicted results will be validated with the elaborated acoustic flight test measurements recently conducted by ECD with the active rotor flap system within the German research project INROS.
Based on this high quality database, it is now possible to perform calculations for a rotor trimmed to the flight test conditions and determine the sensitivity of the acoustic simulation with respect to typical variations of flight and/or higher harmonic control parameters.
The tonal noise components emitted by the main rotor have to be extracted from the recorded acoustic signal to allow a reasonable comparison with the calculation results for a wide range of directivities.
A thus validated simulation model will enhance the understanding of the BVI phenomenon and allow an efficient approach towards the optimisation of higher harmonic control laws and the acoustic benchmarking of active and passive rotor concepts.

Performance

DSF Performance Test Case

For the present investigation a forward flight case with a medium advance ratio of $\mu = 0.3$ was selected. For both the passive and the active rotor the shaft angle was held fixed at α_q=*-4.9°* and the calculations were trimmed for thrust, lateral and longitudinal mast moment by adaptation of the free controls θ_0, θ_{1c}, θ_{1s}. Flight condition and trim objective are summarized in Table 2.
The active ATR-A rotor blade features three adjoining flap segments with a chordwise extent of 15% chord and the radial positions *r/R = 0.69 – 0.75*, *r/R = 0.75 – 0.8* and *r/R = 0.8 – 0.85*. For the present calculations a common control law was used for the innermost and the central flap segment, whereas the outermost segment remains fixed at zero deflection. The 2/rev flap control law is given by:

$$A(t) = A_0 \cdot \cos(2 \cdot \Omega \cdot t - 2 \cdot \varphi) \qquad (3)$$

The flap amplitude was prescribed to A_0 = *6°*. With an increment in azimuth of $\Delta\varphi$ = *30°* for the rotor, a $\Delta\varphi'$ = *60°* resolution of the phase shift in the control law has been investigated.

Table 2: Flight condition and trim objective

Flight speed Mach number	0.21
Blade tip Mach number	0.64
Blade tip Reynolds number	4.7×10^6
Rotor shaft angle	-4.9 deg
Far field pressure	84400 Pa
Far field temperature	279 K
Thrust coefficient	0.008
Rotor mast's pitch moment cf.	-0.69×10^{-4}
Rotor mast's roll moment	-0.21×10^{-4}

Details about the numerical modelling, i.e. mesh size, applied turbulence model can be found in [32].

DSF Performance Results

The investigation of a 2/rev flap control law with respect to the rotor performance, i.e. the required rotor power is presented here. And it will be seen that a relative evaluation of performance can be undertaken with the applied approach.

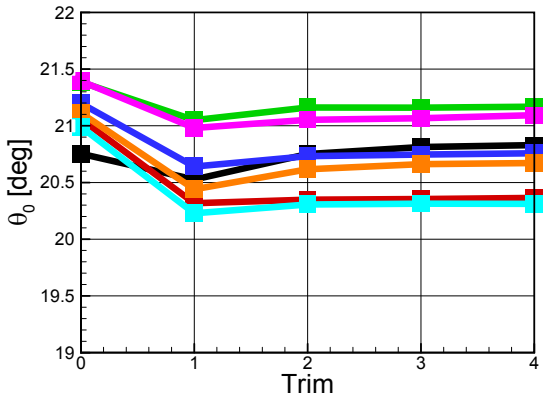

Figure 26: Convergence of collective pitch

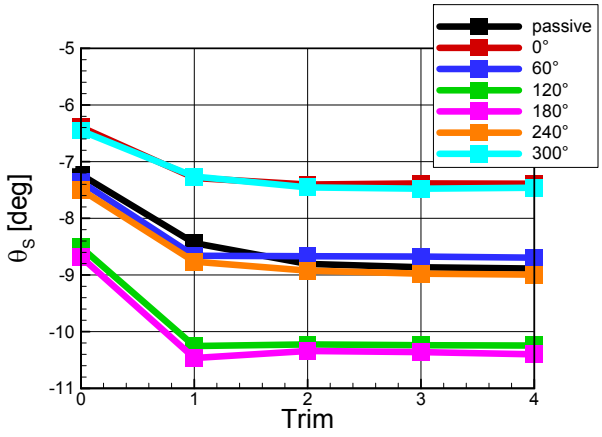

Figure 27: Convergence of lateral cyclic pitch

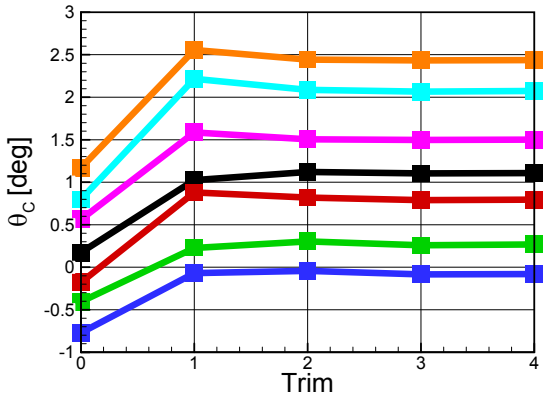

Figure 28: Convergence of longitudinal cyclic pitch

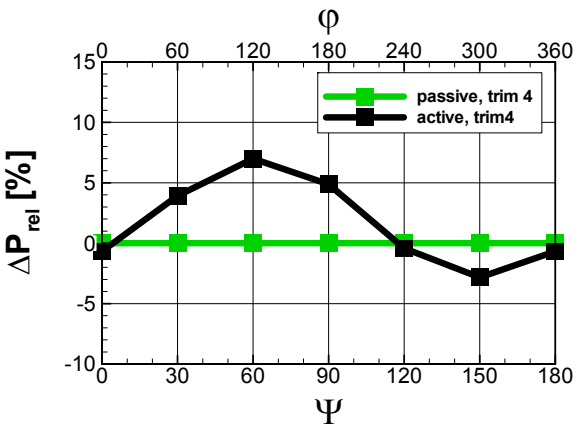

Figure 29: Relative rotor power wrt. the passive rotor

For this purpose, the rotor performance variation has been investigated for six different flap phase angles covering one period of the flap movement with a $\Delta\varphi = 60°$ resolution.

The trim convergence of the control angles θ_0, θ_{1c} and θ_{1s} for all flap phase angles compared to the passive rotor is given in Figure 26 to Figure 28. For all computations all free controls converged to the required accuracy within four re-trim cycles. Even though a systematic deviation of the 0th HOST trim with respect to the final trimmed state can be observed for all three controls, HOST is able to predict the influence of the variation of the flap phase on the rotor trim. All initial HOST computations require a larger (more negative) θ_{1s} input to achieve the required longitudinal mast moment and a slightly higher collective pitch.

The influence of the 2/rev flap control on the rotor performance is depicted in Figure 29. It shows the relative power consumption of the active rotor with respect to the passive rotor for the phase angle variation of the control law. The power consumption of the passive rotor after the 4th trim has been chosen as reference power. The relative power consumption is plotted on y axis, whilst the azimuth increment of the flap phase is given on the lower x axis whereas the 2/rev control phase is given on the upper x axis.

Looking at the phase variation it can be observed that the active rotor consumes in most parts of the phase sweep more power than the passive rotor. Only in the last quadrant a power saving can be observed. The optimum phase is around φ=300°, where the rotor consumes a little less then 3% less than the passive rotor.

This observation is substantiated by the mean values of the unsteady rotor torque. Figure 30 shows the unsteady aerodynamic torque

coefficient around the rotor axis in trimmed state. Since it is a four bladed rotor only, the first quarter is shown. In agreement with the relative power phase plot the calculation with φ=300° shows the lowest mean value, combined with the lowest amplitude.

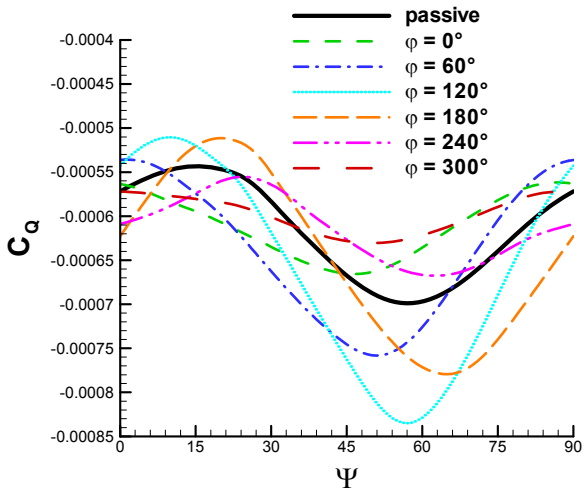

Figure 30: Unsteady aerodynamic torque in trimmed state

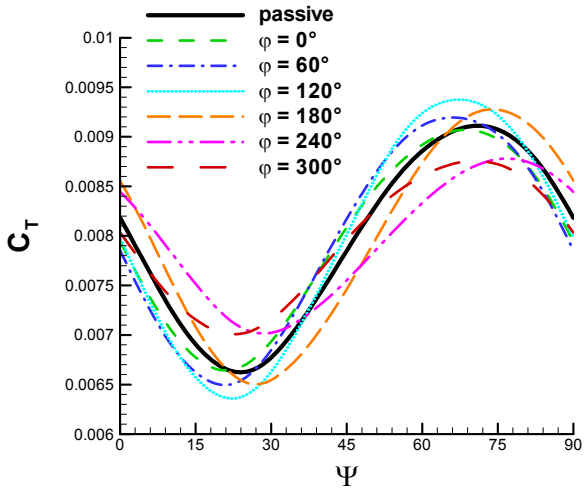

Figure 31: Unsteady aerodynamic thrust in trimmed state

Furthermore, the flap input also affects the unsteady aerodynamic thrust, shown in Figure 31. Although the mean thrust is equal for all phase angles (the calculations were trimmed for thrust), the amplitude of the unsteady rotor thrust may be different. A flap control input with a phase angle of $\varphi = 300°$ results in a significant reduction of the amplitude of the aerodynamic thrust.

The main cause for the thrust variation is the servo flap effect. The flap is deflected and introduces an additional torsion moment about the feathering axis, which consequently changes the thrust over azimuth distribution.

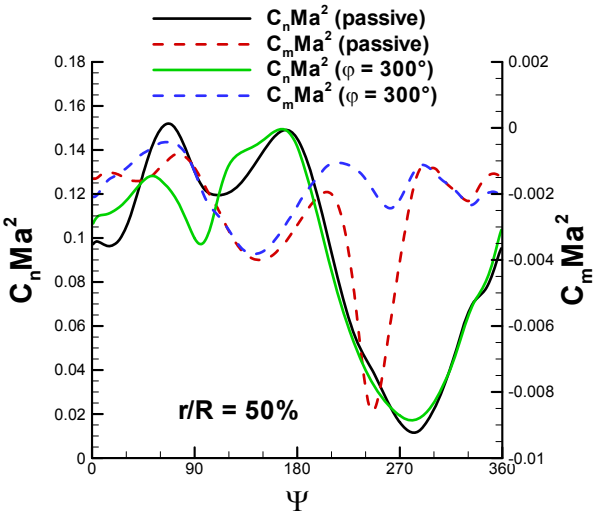

Figure 32: Comparison of C_nMa^2 and C_mMa^2 between active and passive rotor at r/R=0.5

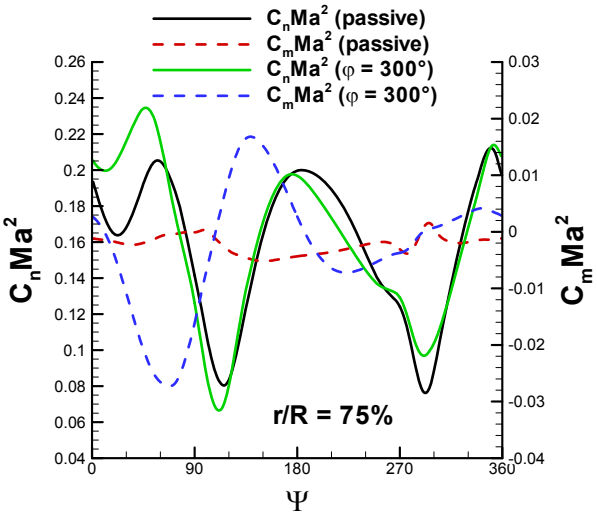

Figure 33: Comparison of C_nMa^2 and C_mMa^2 between active and passive rotor at r/R=0.75

As highlighted above, the flap input with $\varphi = 300°$ phase angle resulted in the minimum power consumption. In this section, a deeper analysis of the passive and the active rotor will be pursued for this phase angle.

Figure 32 and Figure 33 show a comparison between the active and passive rotor for the coefficients C_nMa^2 and C_mMa^2. The radial position *r/R=0.5* (Figure 32) is inboard from the flap region and thus not directly affected by the flap deflection. However, the radial position r/R=0.75 of Figure 33 is located within the flap range. For both radial positions minor differences in C_nMa^2 occur within the second half of the revolution.

More significant differences are observed on the advancing blade side. The downward deflection of the flap at $\psi = 30°$ causes a nose-down twist of the blade. At *r/R=0.5,* C_nMa^2 is reduced compared to the passive rotor due to

this negative twist. At *r/R=0.75,* the effective increase of the airfoil camber due to the flap deflection (and thus the increase of the effective angle of attack) must be taken into account, leading to an increase of C_nMa^2 despite of the nose-down twist. At ψ*=300°,* the opposite is true. The upward deflection of the flap leads to a nose-up elastic twist, which increases C_nMa^2 at *r/R=0.5*. At *r/R=0.75* the airfoil's effective angle of attack is reduced by the flap deflection, resulting in a lower value of C_nMa^2. Note the large influence of the flap deflection on the pitching moment, especially on the advancing blade side.

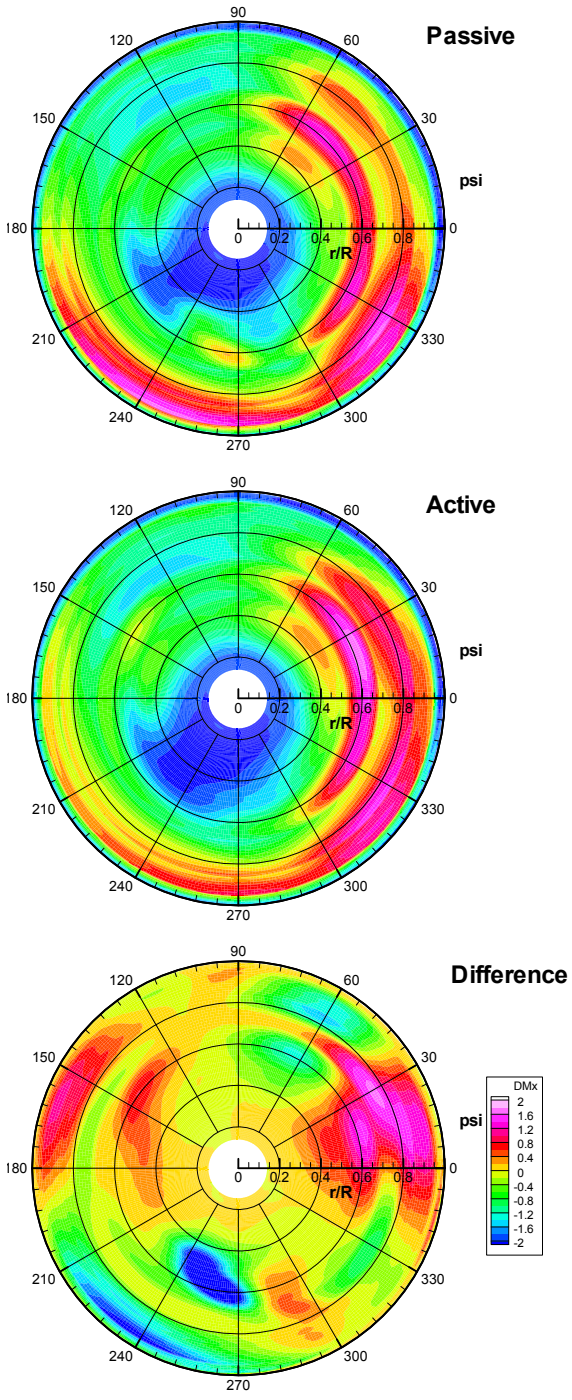

Figure 34: Torque distribution over rotor disk

The torque distribution (Mx in FLOWer convention) on the rotor disk is given in Figure 34. Here red regions indicate high torque contributions of the radial sections and dark blue regions a propulsive torque in the rotor plane. The colour coding in the difference plot shows torque reductions for the active rotor in blue and torque increase in red.

Changes in the drag distribution can be observed on the whole rotor disk. Here again, the flap range of the active rotor can be identified as a ring-shaped area which is separated from the inner and outer radial regions by a discontinuity in drag related torque. This can be explained by the fact that an upward deflection of the flap (ψ=150° and ψ =330°) results in a reduction of the effective airfoil camber and thus, a torque reduction (red/orange areas). Whereas a downward deflection (ψ=60° and ψ=240°) increases the camber and therefore the drag (green areas).

Again the changes on the retreating side are remarkable, since the simulations reproduce the impact of the 2/rev control law on retreating blade stall even though a standard two equations turbulence model is applied.

Over the rotor disk, areas of increased and reduced drag can be found. The influence on the mean value is thus hard to determine. But as seen from the previous section, the mean drag must have slightly decreased, as the mean rotor torque has decreased by nearly 3%.

DSF Flight Speed Sweep with Optimum Phase Angle

The results from the previous section have shown that the minimum power consumption is obtained at a flap phase angle of φ*=150°*. Furthermore, it has been shown that the effect of the reduction of required rotor power is related to the positive influence of active control on the flow separation on the retreating blade side. Hence, it can be expected that the potential of active control with respect to power reduction increases with the increase of non-linear flow effects, i.e. with increasing flight speed and rotor loading. Therefore the influence of a flight speed variation on the rotor performance has been investigated. The phase angle of the control law has been held fixed at the optimum value of φ*=150°* since a phase sweep at 160kts flight speed revealed the same optimum phase angle of φ*=150°*.

The results presented in this section have been obtained for a helicopter with a reduced take-off weight at a lower flight level. Hence the rotor loading is reduced compared to the trim

condition used for the investigations of the previous section. Nevertheless, it can be assumed that the results with respect to the flight speed variation remain valid and the tendency can be directly transferred towards a higher rotor loading.

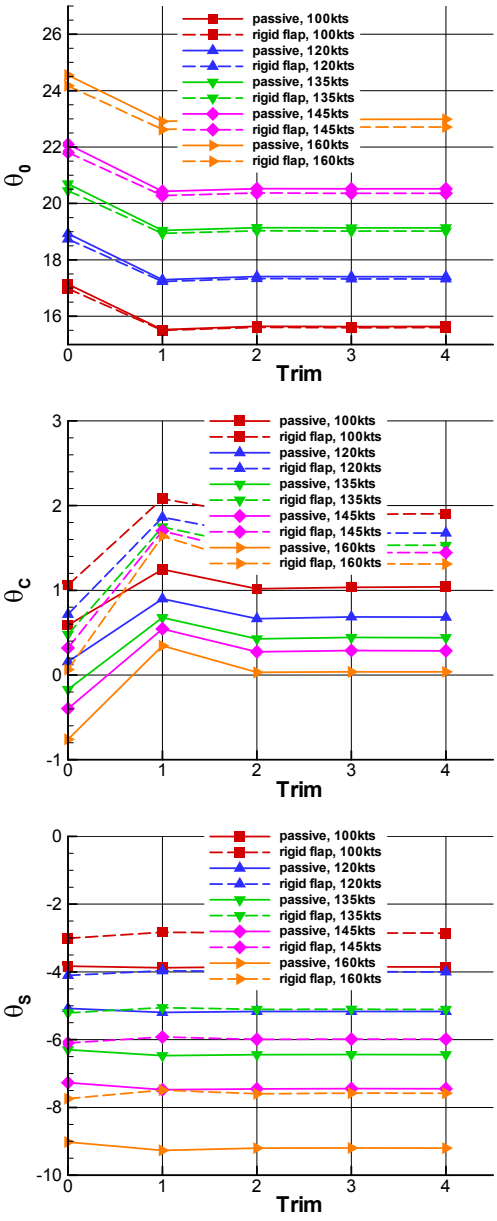

Figure 35: Convergence of collective and cyclic pitch angles

Figure 35 shows the trim convergence of the control angles for the investigated flight speeds of 100kts, 120kts, 135kts, 145kts and 160kts. It can be seen that again very good convergence properties have been obtained, even for the highest flight speed at 160kts.
In Figure 36 the relative power consumption of the active rotor compared to the passive one at the same flight speed is plotted versus the flight speed. Both the result of the 0th HOST trim (no CFD) and the coupled CFD/CSD solution are shown.

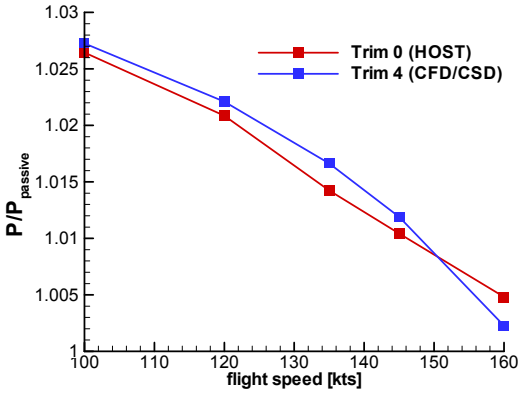

Figure 36: Relative power consumption, reference power: passive rotor at same speed

The relative increase in power consumption decreases with the flight speed. Note, that the coupled CFD/CSD solution predicts a higher power increase than the stand-alone HOST solution for all flight speeds from 100kts to 145kts. At 160kts things look different: Here, the coupled solution predicts a lower power increase which exceeds the power consumption of the passive rotor by only 2%.

Thus, we can conclude as follows:

- The potential of active control increases with increasing flight speed, as non-linear flow effects become more dominant.
- The CFD solution is likely to improve the predicition of such non-linear effects

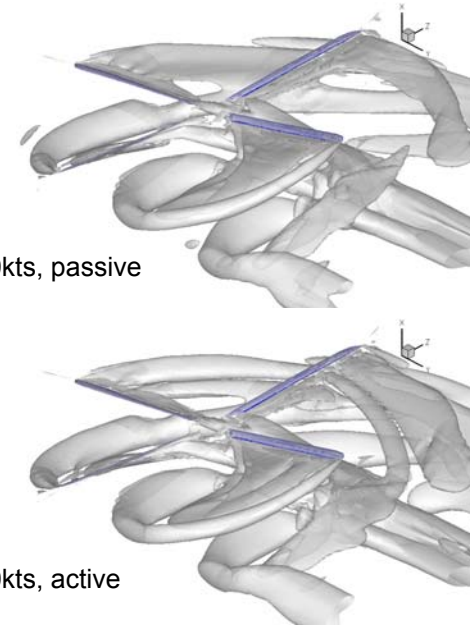

160kts, passive

160kts, active

Figure 37: Visualization of 3D flow field for active and passive rotor at 160kts

Figure 37 shows exemplarily the 3D flow field obtained for the passive and active rotor at

160kts flight speed. The pictures emphasize the high complexity of the resulting flow fields and substantiate the need to introduce nonlinear aerodynamic modelling into the coupled aerodynamic/dynamic rotor solution.

ATE Performance Results

In this section we present first results that have been obtained for the flap configuration used in the FRIENDCOPTER project. In contrast to the LARS project the discrete trailing edge flap is replaced by a continuous deflection of an elastic trailing edge. The active rotor blade features one elastic trailing edge segment with a chordwise extent of 20% chord and the radial position *r/R = 0.56 – 0.91*. Hence, the radial extension of the actuated blade part is approximately three times larger than in case of the LARS configuration. At the radial borders the deflection of the trailing edge is continuously reduced towards zero within a smoothing range of 0.2m. Amplitude of 1.5mm trailing edge deflection has been used for the investigation. Both flap control law and flight condition have been adopted from the flight case presented in the first results section. Note, that the HOST dynamic blade model was modified in order to match the actual FRIENDCOPTER blade properties.

The trim convergence of the control angles is given in Figure 38. It can be seen that the convergence properties have deteriorated compared to our previous investigations using the LARS flap geometry. This is likely to be caused by the larger spanwise extension of the flap, leading to an increased control authority. Figure 38 shows that convergence is poorest for the flap phase angles of φ*=30°* to φ*=90°*. As we will show further below these phase angles lead to the maximum power increase compared to the passive rotor. Hence, the poor convergence behaviour is likely to be caused by an unstable dynamic excitation of the blade. Good convergence has been achieved for the passive rotor and the remaining flap phase angles. This is confirmed by Figure 39 which proves that the passive rotor and the active rotor at φ*=150°* have actually been trimmed towards the same state with an acceptable accuracy.

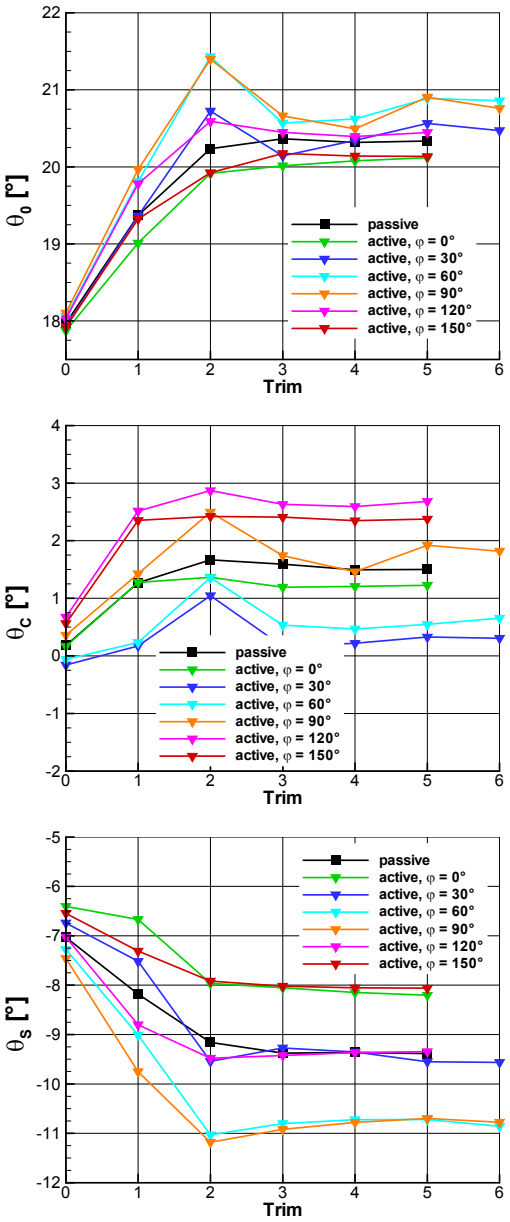

Figure 38: Convergence of collective and cyclic pitch angles

Figure 40 and Figure 41 show comparisons between the 2D HOST loads and the CFD loads, both given in trimmed state for the active rotor at φ*=150°* phase angle. Figure 40 shows the radial distribution of thrust and pitching moment at ψ*=60°* (maximum downward flap deflection), whereas the azimuthal distribution at *r/R = 0.75* (within the flap area) is compared in Figure 41. The Figures show that the 2D and 3D load prediction generally match quite well. As expected the CFD loads show a smoother distribution of the loading in the smoothing range of the spanwise flap boundaries.

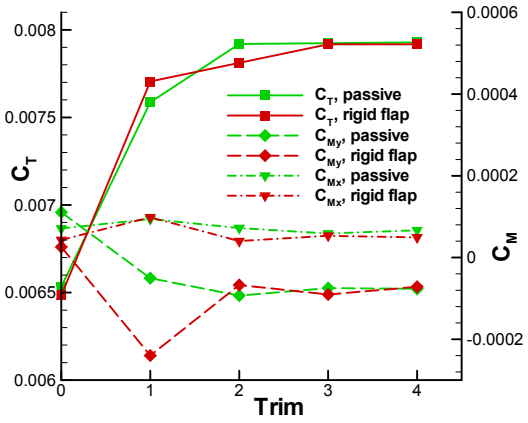

Figure 39: Mean values of rotor load coefficients versus trim iteration

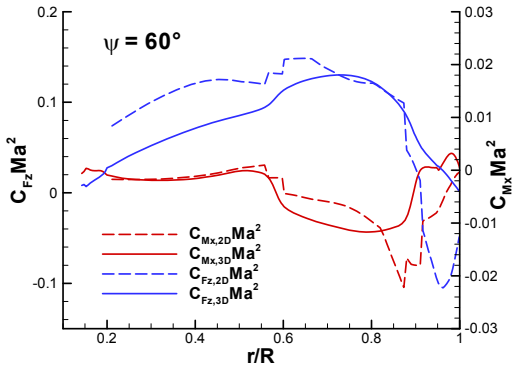

Figure 40: Comparison between HOST loads and CFD loads in trimmed state, $\psi=60°$

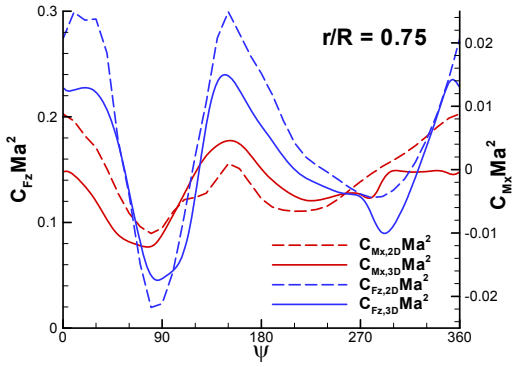

Figure 41: Comparison between HOST and CFD loads in trimmed state, *r/R = 0.75*

Finally, Figure 42 shows the relative power consumption of the active rotor compared to the passive one, both for the 0th HOST trim and in trimmed state. One can see, that both HOST and the coupled solution predict a roughly 1.5% power increase in the optimum phase angle. The initial HOST trim predicts an optimum phase angle of $\varphi=90°$, which constitutes a conspicuous deviation from the previous findings for the LARS flap configuration. The CFD solution corrects the optimum phase angle to the value of $\varphi=150°$, which coincides with the one obtained for the LARS flap geometry.

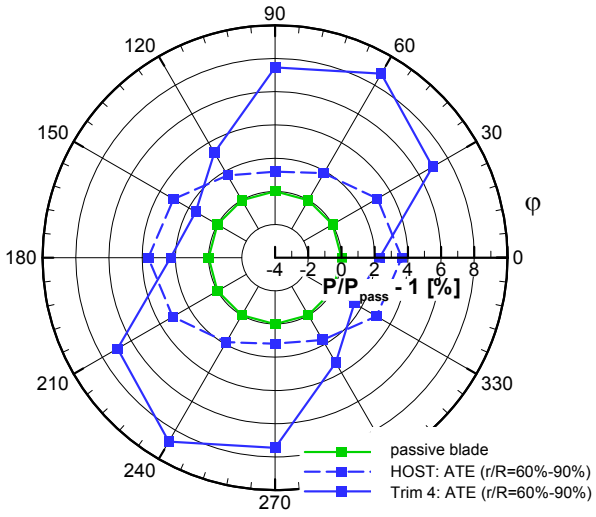

Figure 42: Rotor power over phase angle; ATE in FRIENDCOPTER configuration 20% chord and 60% to 90% radial extension.

Once again, according to Figure 42, no performance gain is realisable with the FRIENDCOPTER configuration. However, by reducing the radial extension of the active region of the ATE to the one of the DSF, i.e. from 70% to 85% span, a performance gain can realised also with the ATE. Figure 43 shows that this gain is slightly smaller than for the DSF. In addition, the penalties off the optimum phase are much higher than for the DSF. This fact indicates that aerodynamic behaviour of the active cross section is different.

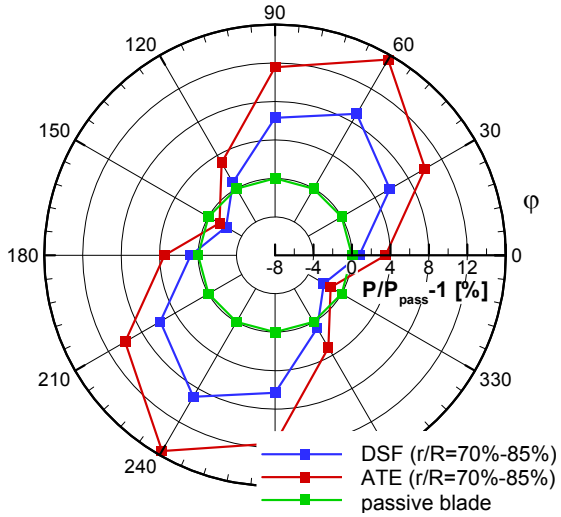

Figure 43: Rotor power over phase angle; red – DSF c=15%, r/R=70%-85%; blue – ATE c=20%, r/R=70%-85% (cf. FRIENDCOPTER configuration with r/R=60%-90%)

Recall Figure 9 and Figure 15: At the same trailing edge position, the tangential angle is much higher for the ATE. Although this produces an increased pitching moment, the drag increases too. Subsequently, a control setting for performance benefit of a highly loaded rotor may not only vary in the used frequencies and phases but also in varying radial portions of the active region.
Acknowledging that DSF and ATE alter the airfoil shape whereas ATW and IBC/2SP do not may help to produce even higher performance benefits with such devices. This is subject of ongoing investigations. However, the authors believe that there is still room for improvement concerning cross sectional shape variation.

Future Trends and Outlook

Noise
Starting from the very encouraging noise benefit demonstration in flight with a 2/rev blade root control on a BO105 [2], [6] that has been confirmed on a modern rotor during flight tests with the discrete active rotor flap system on a BK117, ECD has developed a high level of experience in the field of active rotor control.
Along with the hardware, the numerical simulation techniques have also been largely improved over the years and are now at the edge of becoming efficiently applicable in the industrial design process.
In short term the main challenge will be the detailed analysis of an extensive flight test program with the discrete rotor flap system recently performed by ECD. Based on this rich database a thorough validation of the acoustic tool chain with focus on the 2/rev control is necessary to identify the main influence parameters for active noise control.

A thus validated prediction capability is the key to assess the most promising design concept and improve the performance of the active control in order to exploit the full noise reduction potential offered by an active rotor system.
Aside from the BVI noise abatement the flexibility of the 2/rev control allows a wider range of further applications. A reduction of high speed impulsive noise in fast forward flight is for example as well conceivable as a purposive manipulation of the noise emission directivity characteristic of a helicopter in descent flight. Especially the latter could become a major advantage in the increasingly important land use planning topic.

Performance
It is planned for the near future to validate the shown gains of up to 4% by flight tests with the active flap rotor.
As shown in the paper performance gains will be realised more easily for highly loaded rotor at the boundary of the flight envelope of the helicopter.
Improving the concepts of airfoils shape change with respect to drag or even changing to other concepts like active twist (ATW) that keep the wing aerodynamically clean might further improve the possibility to realise performance gains.
Finally, it is important to note that also other benefits can be tackled by active rotors like dynamic blade and pitch link loads.

Global perspective
Looking to the global benefit for the helicopter, active rotor control provides a clear potential for improvement in several areas:

- More comfort by vibration reduction (not addressed in this paper)
- Reduction of the external noise emission, especially during descent flight condition.
- Reduction of power required respectively fuel consumption: Small reduction evaluated in this paper due to the limited flight envelope, but a clear potential for future scenarios.

However, an increased benefit especially on the domain of performance, but also on the domain of noise and vibration and further domains (e.g. reduction of rotor loads) has to be demonstrated in order to strengthen the arguments for an active rotor control system, which implies additional complexity, weight and cost compared to the conventional rotor.
In the near future, especially the requirements for larger reduction of fuel consumption may make the performance topic respectively the fuel reduction topic to the most decisive one. In order to achieve more progress in this context, the control of the rotor blade geometry itself has to be envisaged as well. Beside the “adaptive airfoil contour topic”, which is today more vision than reality, the steady blade twist and higher harmonic blade twist control laws seem to provide the largest potential. Some industrialisation aspects with regard to actuation principle and blade design constraints have still to be solved, but this scenario is for sure the most promising one for performance improvements, respectively the reduction of fuel consumption. The combination of the objectives

of the “green helicopter” with an acceptable industrial solution may be the most promising concept for a mid term perspective.

Acknowledgments

The authors would like to thank the German ministry of Economy and Labour (BMWA) for its funding in the framework of CHANCEII, LARS and INROS as well as the European Union for its funding in the framework of FRIENDCOPTER.

References

[1] Schimke, D., Arnold, U, and Kube, R.: *“Individual Blade Root Control Demonstration Evaluation of Recent Flight Tests.”* American Helicopter Society 54th Annual Forum, Washington, DC, May 20-22, 1998.

[2] Schöll, E., Gembler, W., Bebesel, M., Splettstößer, W., Kube, R., Pongratz, R.: *“Noise Reduction by Blade Root Actuation - Analysis of Flight and Wind Tunnel Tests.”*, 24th European Rotorcraft Forum, Marseille, France, September 15-17, 1998.

[3] Kloeppel, V., Enenkl, B., and Strehlow, H.: *”Rotor Blade Control by Active Helicopter Servo Flaps.”* International Forum on Aeroelasticity and Structural Dynamics 2005, Munich, Germany, June 2005.

[4] Roth, D., Enenkl, B., and Dieterich, O.: *“Active Rotor Control by Flaps for Vibration Reduction - Full scale demonstrator and first flight test results.”* 32nd European Rotorcraft Forum, Maastricht, the Netherlands, September 2006.

[5] Dieterich, O., Enekl, B., and Roth. D*.: ”Trailing Edge Flaps for Active Rotor Control Aeroelastic Characteristics of the ADASYS Rotor System.”*, American Helicopter Society 62nd Annual Forum, Phoenix, AZ, May 9-11, 2006.

[6] Bebesel, M., Roth, D., and Pongratz, R.: *“Reduction of BVI Noise on Ground – In-Flight Evaluation of Closed-Loop Controller.”* 28th European Rotorcraft Forum, Bristol, UK, September 2002.

[7] Roth, D.: *“Advanced Vibration Reduction by IBC Technology.”* 30th European Rotorcraft Forum, Marseille, France, September 2004.

[8] Enenkl, B., Köppel, V., Preißler, D., and Jänker, P.: *“Full Scale Rotor with Piezo-electric Actuated Blade Flaps.“* 28th European Rotorcraft Forum, Bristol, United Kingdom, September 2002.

[9] Grohmann, B., Maucher, Ch., Prunhuber, T., Jänker, P., Dieterich, O., Enenkl, B., Bauer, M., Ahci, E., Altmikus, A., and Baier, H.: *“Multidisciplinary Design and Optimisation of Active Trailing Edge for Smart Helicopter Rotor Blade.”,* First international symposium on design modelling and experiments of adaptive structures and smart systems, DEMEASS 1, Turin, Italy, 2006.

[10] Grohmann, B., Maucher, Ch., and Jänker, P.:*”Actuation Concepts for Morphing Helicopter Rotor Blades.”*, 25th International Congress of the Aeronautical Sciences, ICAS, Hamburg, Germany, September 2006.

[11] Grohmann, B., Maucher, Ch., Jänker, P., Altmikus, A., and Schimke, D.: “Aero-servo-elastic Pre-design of a Smart Trailing Edge Tab for an Adaptive Helicopter Rotor Blade.”, CEAS/AIAA/DGLR International Forum on Aeroelasticity and Structural Dynamics Munich, Germany, June 2005.

[12] Maucher, Ch., Grohmann, B., Jänker, P., Altmikus, A., Jensen, F., and Baier, H.: “ Actuator Design for the Active Trailing Edge of a Helcopter Rotor Blade.”, 33rd European Rotorcraft Forum, Kazan, Russia, September 2007.

[13] Ahci, E., and Pfaller, R.: “Structural Design, Optimization and Validation of the Integrated Active Trailing Edge for a Helicopter Rotor Blade.”, American Helicopter Society 64th Annual Forum, Montreal, Canada, April 29-May 1, 2008.

[14] Masarati, P., Morandini, M., Riemenschneider, J., Wierach, P., Gluhih, S., and Barkanov, E.: *”Optimal Design of an Active Twist 1:2.5 Scale Rotor Blade.”*, 31st European Rotorcraft Forum, Florence, Italy, September 13-15 2005.

[15] Wierach, P., Riemenschneider, J., Opitz, S., and Hoffmann, F.:” Experimental Investigation of an Active Twist Model Rotor Blade under Centrifugal Loads.”, 33rd European Rotorcraft Forum, Kazan, Russia, September 2007.

[16] Johnson, W., *“Comprehensive Analytical Model of Rotorcraft Aerodynamics and Dynamics”,* Vol. I – VII. Johnson Aeronautics, Sept. 1998.

[17] Johnson, W., *“Rotorcraft Aerodynamic Models for a Comprehensive Analysis”,* American Helicopter Society 54th Annual Forum, Washington, DC, May 1998.

[18] Yin, J., Delfs, J.: *"Improvement of the DLR Rotor Aeroacoustic Code (APSIM) and its validation with Analytic Solution"*, 29th European Rotorcraft Forum, Friedrichshafen, Germany, 2003.

[19] Yin, J., Buchholz, H., and Splettstoesser, W., *"Numerical Simulation of Bo105 Main/Tail Rotor Interaction Noise and Preliminary Comparisons with Flight Test Results"*, 28th European Rotorcraft Forum, Bristol, England, 17 - 20 Sep. 2002.

[20] Lim, J. W. et. al., *"HART-II: Prediction of Blade-Vortex Interaction Loading,"* 29th European Rotorcraft Forum, Friedrichshafen, Germany, September 16-18, 2003.

[21] Pidd, M., Dummel, A., Falchero, D., Genito, M., Prospathopoulos, J., Visingardi, A., Voutsinas, S., G., Yin, J.: *"Validation of Aeroacoustic Predictions using the HeliNovi Database"*, 32nd European Rotorcraft Forum, Maastricht, the Netherlands, September 2006.

[22] Toulmay, F., Arnaud, G., Falchero, D. and Villat, V.: *"Analytical Prediction of the Rotor Dynamics for Advanced Geometry Blades",* American Helicopter Society, 52nd Annual Forum, Washington, D.C., June 1996.

[23] Benoit, B., Dequin, A-M., Kampa, K., Grünhagen, W. v., Basset, P-M., Gimonet, B.: *"HOST: A General Helicopter Simulation Tool for Germany and France",* American Helicopter Society, 56th Annual Forum, Virginia Beach, Virginia, May 2000.

[24] Kroll, N., Eisfeld, B. and Bleecke, H.M., "*The Navier-Stokes Code FLOWer",* Volume 71 of Notes on Numerical Fluid Mechanics, pages 58-71. Vieweg, Braunschweig, 1999.

[25] Jameson, A., Schmidt, W. and Turkel, E.: *"Numerical Solutions of the Euler Equations by Finite Volume Methods Using Runge-Kutta Time-Stepping Schemes",* AIAA-Paper 81-1259, 1981.

[26] Jameson, A.: *"Time Dependent Calculation Using Multigrid, With Applications to Unsteady Flows Past Airfoils and Wings",* AIAA-Paper 91-1596, 1991.

[27] Pahlke, K. G.: *"Berechnung von Strömungsfeldern um Hubschrauberrotoren im Vorwärtsflug durch die Lösung der Euler-Gleichungen",* DLR-Forschungsbericht 1999-22, ISSN 1434-8454, 1999.

[28] Altmikus, A. R. M. and Wagner, S.: *"CHANCE - Complete Helicopter Advanced Computational Environment: WP 4.2 Full Coupling and Trim"* 2. Advancement Report, Reporting Period: 01.01.2000 - 31.12.2000, Institut für Aero- und Gasdynamik, Universität Stuttgart, 2001.

[29] Servera, G., Beaumier, P., Costes, M.: *"A weak coupling method between the dynamics code HOST and the 3D unsteady Euler code WAVES"*, 26th European Rotorcraft Forum, The Hague (The Netherlands), Sept. 2000.

[30] Altmikus, A. Wagner, S., Beaumier, P., Servera, G.: *"A Comparison: Weak versus Strong Modular Coupling for Trimmed Aeroelastic Rotor Simulations",* American Helicopter Society 58th Annual Forum, June 2002.

[31] Dietz, M., Krämer, E., Wagner, S., and Altmikus, A..: "Weak Coupling for Active Advanced Rotors.", 31st European Rotorcraft Forum, Florence, Italy, September 13-15 2005.

[32] Altmikus, A., and Knutzen, B.: *„Trimmed Forward Flight Simulation with CFD featuring Elastic Rotor Blades with and without Active Control"*, American Helicopter Society 63rd Annual Forum, Virginia Beach, VA, May 2007.